DOI: 10.1002/ejic.200600298

Crystal Structure and Properties of $MgCo_4Ge_6$

Christine Gieck,[a] Martin Schreyer,[a] Thomas F. Fässler,*[a] Fabian Raif,[b] and Peter Claus[b]

Keywords: Intermetallic phases / Germanium / Heterogeneous catalysis / ELF (Electron Localization Function) / Density functional theory

$MgCo_4Ge_6$ is a novel compound in the ternary system Mg-Co-Ge. Single crystals for a structure analysis were obtained from mixtures of the elements at high temperatures in sealed tantalum ampoules. The tetragonal structure [$I\bar{4}_2m$; a = 6.1725(9) and c = 8.660(2) Å; YRu_4Sn_6 structure type] was determined by X-ray single crystal analysis and refined to R_1 = 0.027 for all data. The electronic structure is discussed by means of density of states and band-structure analyses on the basis of density functional theory. Chemical bond analysis is performed using the electron localization function (ELF). The catalytic properties of the polar intermetallic alloy with respect to the selective hydrogenation of α,β-unsaturated aldehydes are discussed and compared with those of the recently investigated $MgCo_6Ge_6$.

Introduction

The synthesis of polar intermetallic alloys with a well-defined stoichiometry is attempted in order to obtain substitutes for the expensive platinum group metal catalysts currently used for the selective hydrogenation of α,β-unsaturated aldehydes. While both the electronic and structural properties of intermetallic compounds, as well as the catalytic properties of some alloys on ceramic supports, have been studied extensively, no systematic investigations on the catalytic properties of well-defined alloys have been reported yet. A comparison of the ternary tetrelides of cobalt and ruthenium shows that isotypic compounds are obtained in many cases.[1–4] Besides this isotypic relationship, which can be taken as evidence for the similarity of the chemical properties of the two metals involved, we have also found that specific element combinations in alloys lead to an unexpected catalytic activity. In this context, we have recently reported the catalytic properties of Mg_2Sn[5] and $MgCo_6Ge_6$,[6] both of which show a remarkable activity and a high selectivity for the hydrogenation of *cis*/*trans* citral to geraniol and nerol. Since alloys of such compositions have not yet been considered as catalytically active materials, we extended our systematic study to other compounds in the ternary phase diagram Mg-Co-Ge and report here on the novel representative $MgCo_4Ge_6$.

[a] Department Chemie, Technische Universität München, Lichtenbergstr. 4, 85747 Garching, Germany
Fax: +49-89-289-13186
E-mail: thomas.faessler@lrz.tum.de
[b] Ernst-Berl-Institute/Chemical Technology II, Department of Chemistry, Technical University Darmstadt, Petersenstr. 20, 64287 Darmstadt, Germany

Results and Discussion

Crystal Structure

$MgCo_4Ge_6$ crystallizes in the YRu_4Sn_6 structure type and can be derived from the Au_3Cu structure.[7,8] The relationship between the structure of $MgCo_4Ge_6$ and that of Au_3Cu is emphasized in Figure 1. The Au_3Cu structure derives from a cubic close packing of Au atoms by replacing every fourth Au by a Cu atom in each close packed layer, whilst maintaining the Au triangles. The cubic packing of those trigonal layers labeled as A, B, and C is shown in Figure 1 (a). Replacement of every second Mg atom in the hypothetical, corresponding $MgGe_3$ structure by a C_{2v} distorted tetrahedral Co_4 unit in an ordered manner (Figure 1, b) leads to the title compound (Mg_2Ge_6 → $MgCo_4Ge_6$). In the Au_3Cu structure, Cu is cube-octahedrally coordinated by 12 Au atoms, and in $MgCo_4Ge_6$ Mg is similarly coordinated by 12 Ge atoms, although in a strongly distorted cube-octahedral manner. Two opposite squares of the six present in a cube-octahedron are rhomboidally distorted, with the orientation of the two short diagonals perpendicular to each other. The lengths of the short diagonals are in the range of the other Ge–Ge contacts within the cube-octahedron. The rhomboidal distorted squares of the Ge_{12} cube-octahedra are strongly bent, thereby retaining the convex nature of the polyhedron. The remaining four squares of the cube-octahedron are capped by Co atoms. The resulting 16-vertex polyhedron $Mg@Ge_{12}Co_4$ is shown in Figure 2 (a). These polyhedra form a tetragonal body-centered packing and are interconnected by common vertices and external Co–Co bonds (Figure 2, b).

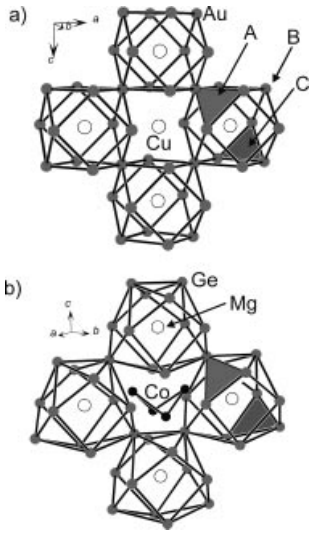

Figure 1. The relation between the $MgCo_4Ge_6$ and the Au_3Cu structure. a) The Au_3Cu structure; labels indicate atoms and the cubic stacking sequence of the layers A, B, and C; the Au_3 triangles of each layer are highlighted in grey. b) Related packing of $MgGe_{12}$ polyhedra in $MgCo_4Ge_6$, with inserted Co_4 units in black.

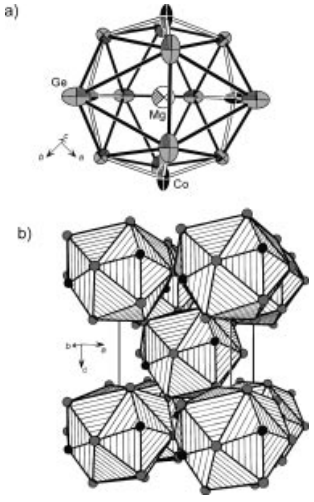

Figure 2. a) The $Ge_{12}Co_4$ coordination polyhedron around the Mg atom. All thermal ellipsoids are shown at 90% probability. b) Tetragonal body-centered packing of $Ge_{12}Co_4$ polyhedra (Co in black, Ge in grey).

An alternative description arises from the Ge sub-lattice, where the connection of the Ge atoms leads to layers of vertex-sharing Ge_8 units in the *ab* plane, with a close analogy between these units and the arrangement in the molecular compound P_4S_4 (Figure 3, a). The Ge substructure forms two-dimensional slabs in the *ab* plane that are stacked in the *c* direction, with each subsequent layer shifted by (1/2, 1/2, 1/2) to form the body-centered packing (Figure 3, b). The P_4S_4-like Ge_8 cages are "filled" with distorted tetrahedral Co_4 units (Figures 3, a and c), and the cavities formed by four vertex-sharing Ge atoms and four bridging Ge atoms host the Mg atoms. The coordination sphere of the Mg atoms is completed by two Ge–Ge contacts of − with respect to the Ge sub-lattice − three-connected Ge atoms of the previous and next Ge layers along the *c* direction (Figure 3, c). The Ge–Ge distances [2.906(1) and 2.987(1) Å] of the Ge sub-structure are longer than in typical covalently connected Ge atoms in Zintl phases, which are about 2.6 Å. Another interesting feature is the Co_4 unit that is present in the P_4S_4-type Ge_8 cages. These show two longer and four shorter Co–Co distances of 3.102(1) and 2.581(2) Å, respectively. The shorter distances

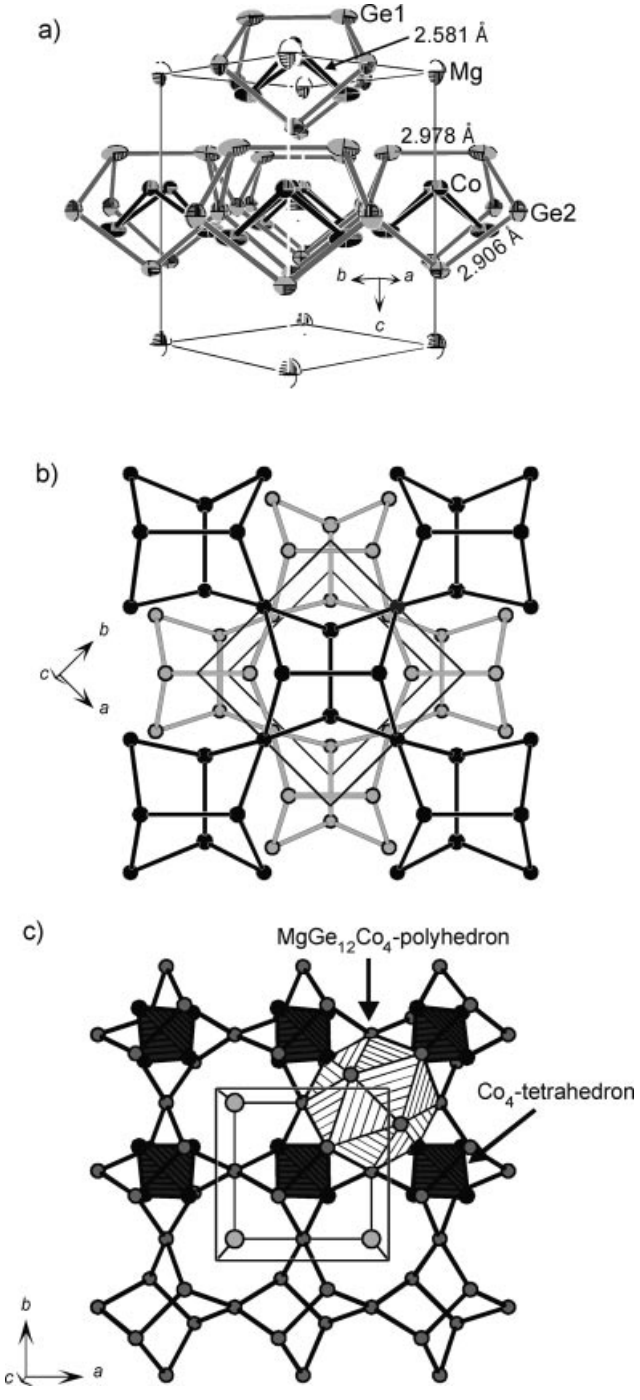

Figure 3. a) Crystal structure of $MgCo_4Ge_6$ as a combination of the Ge substructure centered by Co_4 units. All thermal ellipsoids are shown at 90% probability. b) [001] stacking of the germanium layers. c) Combination of the two views of a) and b).

are close to that observed in α-Co (2.506 Å).[9] Some binary cobalt germanides have even shorter Co–Co contacts, with the shortest being 2.377 Å in Co_5Ge_7.[10] Figure 3 (c) shows the combined picture of the packed polyhedra and the homoatomic Ge substructure: four 16-vertex polyhedra are interconnected in the *ab* plane by four fourfold-connected atoms of one P_4S_4-type Ge_8 entity. Further external interconnections between the polyhedra occur via the shorter Co–Co contacts of the C_{2v} distorted Co_4 tetrahedra.

Catalytic Properties

GC analysis revealed that citral undergoes no conversion in hydrogenation experiments under the reaction conditions described in the Experimental Section (reaction time: 150 min). Therefore, the experiments were repeated with a larger amount of $MgCo_4Ge_6$ (up to 500 mg) under H_2 pressure (7.5 MPa) for a longer reaction time (360 min) in a batch reactor (300 mL, Parr), but again, no conversion was observed. The absence of any catalytic activity is in contrast to the behavior of the intermetallic compound $MgCo_6Ge_6$, for which a citral conversion of 17% was observed at 453 K.[6]

Quantum Chemical Calculations

The TB-LMTO band-structure calculations (Figure 4, a) reveal individual bands with a large dispersion crossing the Fermi level. The Fermi level is located at a local minimum of the density of states (DOS). Thus, $MgCo_4Ge_6$ is clearly a metal with delocalized states at the Fermi level. An analysis of the partial contributions to the DOS shows that the states at the Fermi level have predominantly Co orbital character (Figure 4, b). Ge orbital contributions are located well below the Fermi level, whereas there are virtually no Mg orbital contributions at all. This is consistent with the fact that Mg is the most electropositive element in the compound. The COHP curve in Figure 4 (c) indicates that bonding Ge–Co interactions are optimized up to E_F. Antibonding interactions occur only above E_F. The corresponding COHP curves of Ge–Ge contacts show that these interactions are much weaker. There is a noticeable flat COHP

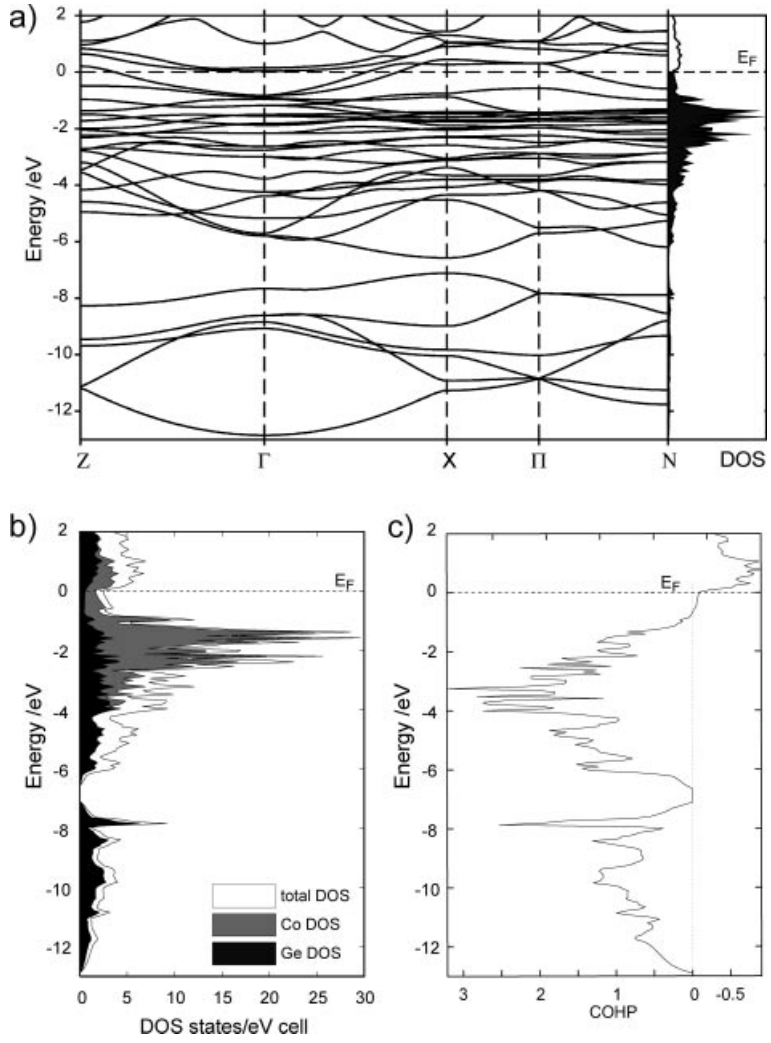

Figure 4. a) Band structure and DOS of $MgCo_4Ge_6$. b) Partial contributions of Co and Ge to the density of states.

region in Figure 4 (c) as well as in the Ge–Ge COHP diagram (not shown) right below E_F. Since there are considerable Ge and Co contributions in the DOS plot of Figure 4 (b) those states must belong to nonbonding states. In order to detect nonbonding domains, chemical bonding was further analyzed by means of the electron localization function (ELF).

Figure 5 shows several two-dimensional cross-sections of the function parallel to the *ab* plane. The color of each pixel corresponds to a certain value of ELF, as illustrated by the color bar at the bottom of Figure 5 (d). Contour lines illustrate ELF isobars and are superimposed onto the pictures. The left-hand column of Figure 5 represents the ELF calcu-

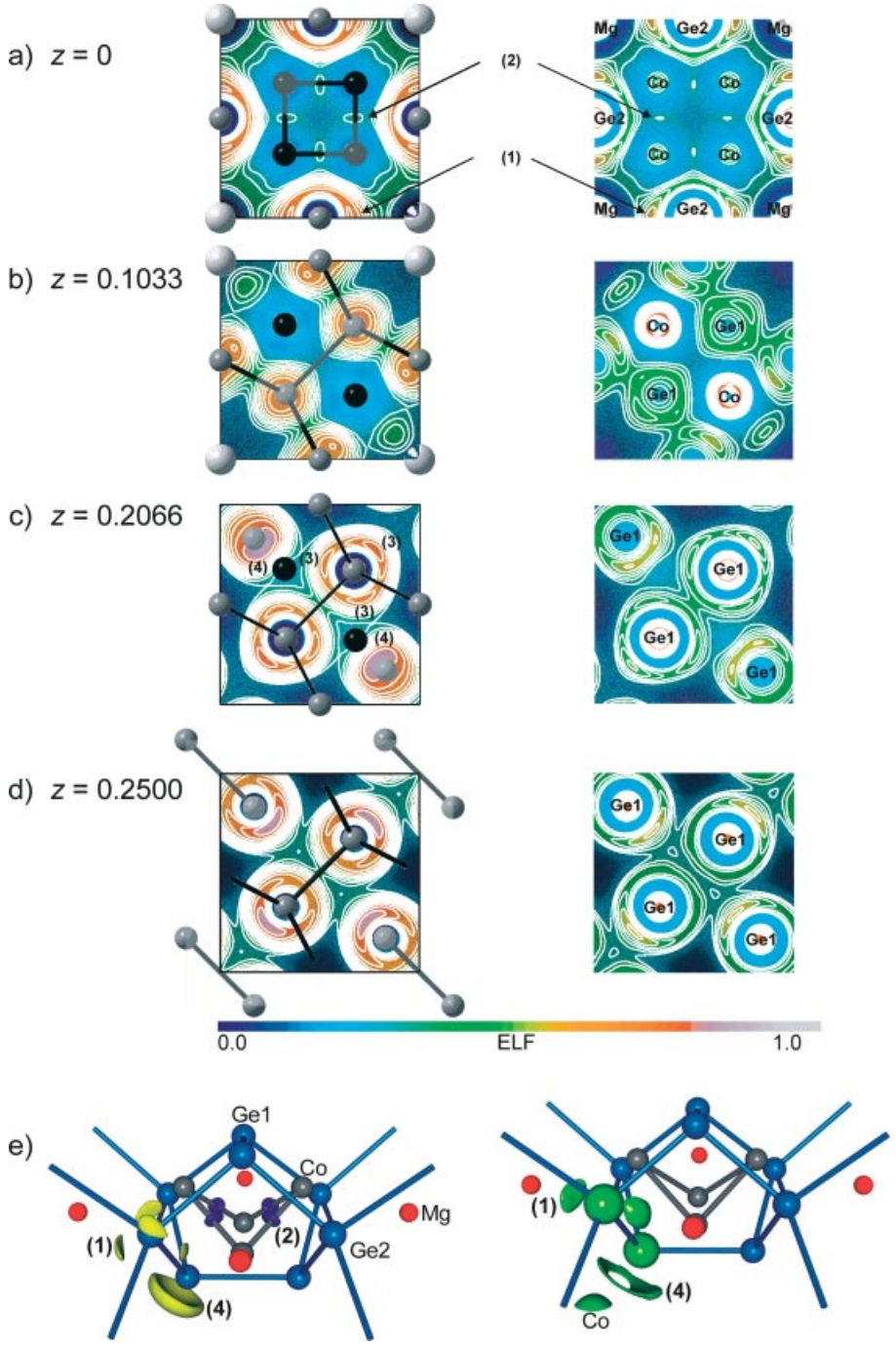

Figure 5. Two-dimensional cross-sections of the ELF in the *ab* plane at different values along the *c* direction. Isobars for $0.3 \leq \text{ELF} \leq 0.8$, with a step width of 0.05, are superimposed on the colored maps. Valence ELF is presented to the left, with all-electron ELF to the right. Structural motifs are superimposed on the valence ELF pictures. e) Left-hand side: 3D Isosurfaces of the ELF around selected atoms. Yellow: valence ELF (ELF = 0.759) at the two germanium sites. Violet: valence ELF (ELF = 0.3) between the cobalt atoms; right-hand side: as in Figure 5 (e), but all-electron ELF (ELF = 0.545 in green) around the germanium sites.

lated from a valence-electron treatment, while the right-hand column illustrates the ELF calculated from the electron density of all electrons, including core electrons. The atoms in the plane and their next neighbors are overlaid. At $z = 0$ the *ab* plane cuts though the Mg and Ge2 atoms and the four centers of the shorter Co–Co bonds of the C_{2v} distorted tetrahedron (Figure 5, a). In both valence and all-electron ELF, maximum values of ELF are observed close to the Ge2 atoms pointing towards the neighboring Mg atoms. The regions (1) can be interpreted as lone-pair-type localization domains since the Ge2 and Mg atoms are ultimately separated by minimum values of ELF. Another small maximum (2) of the function with ELF = 0.3 is observed at the center of the Co–Co bonds, thus indicating a certain degree of covalency for these bonds. The second slice at $z = 0.1033$ (Figure 5, b) cuts through the center of the bonds between the three-connected Ge1 and four-connected Ge2 atoms. No maximum is observed here, and these contacts do not show any covalent contribution. The third cut (Figure 5, c), at $z = 0.2066$, cuts through the Ge1 positions. Three maxima are observed in a staggered position around each Ge1 atom with respect to the three Ge1–Ge2 contacts. Additionally, ELF maxima (4) that can be attributed to the Ge1 atoms of the adjacent layer become visible. In the valence-ELF picture these maxima point directly towards the Co atoms of adjacent layers, while, due to the repulsion between the core and the valence electrons, they appear to be separated into two smaller maxima in the case of the all-electron ELF. Finally, the cut at $z = 0.25$ (Figure 5, d) is located in the middle between two P_4S_4-type layers of Ge_8 cages, where no Ge–Ge bonds can be detected.

The situation in the vicinity of the Ge_8 cages is also outlined in Figure 5 (e), which shows the 3D isosurfaces of the valence ELF to the left and the all-electron ELF to the right. The yellow isosurfaces correspond to an ELF value of 0.76 of the valence ELF. There are five basins and these which must be interpreted as being of a lone-pair type since their ELF maxima are not located on an atom–atom connection vector. The larger one (4) is attached to the Ge1 atom and points away from the three Ge1–Ge2 contacts. Consistent with the 2D images (Figure 5, c) it points towards a Co atom of the adjacent Ge–Co layer. The four smaller, bean-shaped maxima are found around the four-bonded Ge2 atom; the positions of the four local maxima are due to the tetrahedrally oriented Ge2–Ge1 contacts. The valence-ELF isosurface with ELF = 0.3 is superimposed in violet color. The maxima are located at the centers of the shorter Co–Co contacts and confirm a certain degree of covalency, as already deduced from the 2D plots. The right-hand side of Figure 5 (e) shows the all-electron ELF isosurfaces of ELF = 0.545 around the two different germanium sites. The picture differs from that of the valence-ELF: the lone-pair attached to the Ge1 site is significantly flattened as compared to the one in the valence-ELF, and is turned into a crest due to the repulsion of the adjacent cobalt atom by the core electrons. The bean-shaped basins around the Ge2 atoms are contracted to two basins, which are oriented directly towards the adjacent Mg sites.

Conclusions

Our search for other catalytically active alloys in the ternary phase system Mg–Co–Ge has led to the discovery of the novel compound $MgCo_4Ge_6$, which crystallizes in the YRu_4Sn_6 structure type first described by Venturini et al. The structure can be regarded as a coloring of the cubic-close packing observed in the Au_3Cu structure. A closer investigation of the interatomic distances reveals peculiar and unprecedented homoatomic substructures for each of the Ge and Co atoms (Table 1). With respect to the dimensionality of the Ge sub-lattice, the structure is similar to $MgCo_6Ge_6$, which contains a graphite-type Ge sub-lattice with Ge–Ge contacts of about 2.9 Å. Quantum chemical investigations on the DFT level as well as the ELF interpretation of both compounds show that the Ge–Ge contacts of the Ge sub-lattices do not indicate any covalent bond contributions. However, in $MgCo_6Ge_6$ additional Ge_2 dimers with considerably localized bond character in the range of a Ge–Ge single bond were observed. In $MgCo_4Ge_6$ a combination of chemical bond types is found, with the main bonding contributions originating from Co–Ge interactions. ELF analysis reveals lone-pairs at the three-connected Ge atoms of the Ge subnet. These lone-pairs are oriented toward the Co atoms and thus a dative bonding between Ge and Co atoms can be formulated. Further small covalent contributions are found between the transition metal atoms.

Table 1. Interatomic distances [Å] for $MgCo_4Ge_6$.

Ge(1)–Ge(2)	2.906(1) (2×)	Mg(1)–Co(1)	2.894(2) (4×)
Ge(1)–Ge(1)	2.978(1)	Co(1)–Ge(1)	2.285(2)
Co(1)–Co(1)	2.581(2) (2×)	Co(1)–Ge(2)	2.371(1) (2×)
Co(1)–Co(1)	3.102(1)	Co(1)–Ge(1)	2.419(2) (2×)
Mg(1)–Ge(1)	2.945(1) (4×)	Co(1)–Ge(1)	2.469(2)
Mg(1)–Ge(2)	3.086(1) (4×)		

Despite some similarities with respect to chemical bonding properties, such as two-dimensional Ge networks and composition, all attempts to catalyze citral hydrogenation with $MgCo_4Ge_6$ failed, which is in contrast to the catalytic behavior of the intermetallic compound $MgCo_6Ge_6$.[6] This difference indicates that catalytic properties might also depend on the structure type and thus on the electronic properties and not only on the nature of the metals involved.

Experimental Section

Synthesis: $MgCo_4Ge_6$ was synthesized by heating a stoichiometric mixture of the elements in a tantalum crucible to 750 °C for two days, followed by slow cooling of the reaction product to room temperature. The product consisted of xenomorphous crystals with a metallic luster, which were embedded in a microcrystalline silver-metallic matrix. The purity of the sample was established crystallographically, using a STOE STADI P powder diffractometer with a Cu-K_α source. The powder diffractogram, which could be indexed[11] with the help of the theoretical powder pattern calculated for $MgCo_4Ge_6$, showed only slight impurities of elementary Ge.

Crystal Structure Determination: The crystal structure was determined from single-crystal X-ray diffraction data. A single crystal was selected from the reaction mixture and placed into an oil-filled glass capillary. The measurement was performed on a Nonius DIP 2020 diffractometer equipped with a monochromatic Mo-K_α source (λ = 0.71073 Å). Data were collected by a scan of 2° in φ in 180 frames. The exposure time was 300 seconds per frame. The collection of the intensity data was carried out with the HKL2000 program.[12] Cell parameters were initially calculated from reflections taken from five frames of reflections. The final lattice parameters were calculated from all reflections observed in the actual data collection. The data from the data collection were processed with the Scalepack[12] program and corrected for absorption using the PLATON[13] program suite. A summary of the experimental and crystallographic data is given in Table 2.

Table 2. Crystallographic data for $MgCo_4Ge_6$.

Empirical formula	$MgCo_4Ge_6$
Formula weight	695.57
Temperature	293(2) K
Wavelength	0.71073 Å
Crystal system	tetragonal
Space group	$I\bar{4}_2m$
Unit cell dimensions	a = 6.1725(9) Å
	c = 8.660(2) Å
Volume	329.94(9) Å^3
Z	2
Density (calculated)	7.001 g cm^{-3}
Absorption coefficient	36.664 mm^{-1}
F_{000}	624
Crystal size	0.1 × 0.1 × 0.15 mm
Theta range for data collection	4.05 to 27.54°
Index ranges	$-5 \le h \le 5$, $0 \le k \le 8$, $0 \le l \le 11$
Reflections collected	2645
Independent reflections	212
Completeness to θ = 27.54°	100.0%
Absorption correction	PLATON[13]
Refinement method	full-matrix least-squares on F^2
Data/restraints/parameters	212/0/19
Goodness-of-fit on F^2	1.367
Final R indices [$I > 2\sigma(I)$]	R_1 = 0.027, wR_2 = 0.077
R indices (all data)	R_1 = 0.027, wR_2 = 0.077
Largest diff. peak and hole	1.530 and –0.977 e Å^{-3}

The structure was solved by direct methods, which revealed the atomic positions and was refined with the SHELXL-97 program.[14] The final coordinates and equivalent isotropic temperature factors of all atoms are given in Table 3.

Table 3. Atomic coordinates (×10^4) and equivalent isotropic displacement parameters [Å^2 × 10^3] for $MgCo_4Ge_6$. $U_{(eq)}$ is defined as one third of the trace of the orthogonalized U_{ij} tensor.

Atom	Wyck.	x	y	z	$U_{(eq)}$
Mg	2a	0	0	0	20(1)
Co	8i	8223(2)	8223(2)	4215(2)	17(1)
Ge1	8i	8294(1)	8294(1)	7066(1)	18(1)
Ge2	4c	0	5000	0	13(1)

Further details of the crystal structure investigation may be obtained from the Fachinformationzentrum Karlsruhe, 76344 Eggenstein-Leopoldshafen, Germany (Fax: +49-7247-808-666; E-mail: crysdata@fiz-karlsruhe.de) on quoting the depository number CSD-416401.

Hydrogenation Reaction: The hydrogenation of citral (3,7-dimethyl-2,6-octadienal), which has three unsaturated bonds including conjugated C=C and C=O groups as well as an isolated C=C bond, was chosen as a test reaction. Hydrogenation was carried out in a high-pressure batch reactor system described earlier.[15] The reactor was filled with a solution of 1 mL of citral in 9 mL of hexane. After the addition of 100 mg of $MgCo_4Ge_6$ (particle size < 63 mm), the reaction mixture was stirred at 850 rpm, the reactor was flushed four times with argon (2 MPa), and heated up to 453 K within 45 min (0.8 MPa argon pressure was left in the reactor). The reaction was started by setting the hydrogen pressure to 7 or 9 MPa, respectively. Analysis of the reaction mixture by GC (HP 5890, flame ionization detector, DB-WAX capillary column) showed no conversion products.

Quantum Chemical Calculations: The electronic structure was investigated by means of the ab initio full-potential linear muffin-tin orbital (LMTO) method in the atomic sphere approximation (ASA), using the tight-binding (TB) program (TB-LMTO-ASA).[16] The calculations were based on the local-density approximation (LDA), and the Hedin–Lundquist parameterization was employed for exchange and correlation potentials.[17] The radii of the muffin-tin spheres and empty spheres were determined according to Jepsen and Andersen.[18] For the calculations, s, p, and "down-folded" d-partial waves for Ge, s, p, and "down-folded" d-partial waves for Mg, and s, p, and d-partial waves for Co were used. COHP (crystal orbital Hamilton populations) plots[24] show DOS curves, which were weighted by the contributions of each crystal orbital to some measure of the strength of a given bond. The contribution of the covalent part of a particular interaction to the total bonding energy of the crystal can be obtained from COHP analyses. All COHP curves presented here are in the following format: positive and negative values are bonding and antibonding, respectively.

For further insight into the chemical bonding in intermetallic compounds a topographical analysis of the electron density distribution using the Electron Localization Function (ELF), which was originally introduced for the deduction of the shell structure of atoms from the electron density, was performed.[19] ELF values were scaled between 0 and 1, with high ELF values and local ELF maxima corresponding to areas and centers of localized electrons, and low ELF values defining the spatial area around these maxima. The resulting partition of space into areas of high electron localization can be interpreted in terms of bonding and nonbonding electron pairs and reveals their three-dimensional shape. Thus, spatial domains of localized electrons become visible.[20–23] These calculations were carried out both with valence electrons only and with all electrons.

Acknowledgments

This work was supported by the Deutsche Forschungsgemeinschaft (project number FA 198/4-1 and CL 168/3-1: "Polare Legierungen als Mehrkomponenten-Katalysatoren"). The authors would like to thank Dr. Annette Schier for her help with the correction of the manuscript.

[1] Tb_2CoGe_2: O. I. Bodak, V. K. Pecharskii, P. K. Starodub, P. S. Salamakha, O. Ya. Mruz, V. A. Bruskov, *Izv. Akad. Nauk SSSR, Met.* **1986**, *4*, 214–216.
[2] Tb_2RuGe_2: P. Boulet, F. Weitzer, K. Hiebl, H. Noel, *Physik* **2000**, *292*, 302–319.
[3] $Sc_3Co_2Si_3$: E. I. Gladyshevskii, B. Ya. Kotur, *Kristallografiya* **1978**, *23*, 946–950.

[4] $Ho_3Ru_2Ge_3$: O. L. Sologub, Yu. M. Prots, P. S. Salamakha, O. I. Bodak, *J. Alloys Compd.* **1994**, *209*, 107–109.
[5] P. Claus, F. Raif, S. Cavet, S. Cemirel-Gülen, M. Schreyer, T. F. Fässler, *Catal. Commun.* **2006**, *7*, 618.
[6] C. Gieck, M. Schreyer, T. F. Fässler, S. Cavet, P. Claus, *Chem. Eur. J.* **2006**, *12*, 1924–1930.
[7] R. Pöttgen, R.-D. Hoffmann, E. V. Sampathkumaran, I. Das, B. D. Mosel, R. Müllmann, *J. Solid State Chem.* **1997**, *134*, 326–331.
[8] G. Venturini, B. Chafik El Idrissi, J. F. Marêché, B. Malaman, *Mater. Res. Bull.* **1999**, *25*, 1541.
[9] A. Taylor, R. W. Floyd, *Acta Crystallogr.* **1950**, *3*, 285–289.
[10] E. Stolz, K. Schubert, *Chem. Erde* **1962**, *22*, 709–711.
[11] W. Kraus, G. Nolze, *J. Appl. Crystallogr.* **1996**, *29*, 301–303.
[12] Z. Otwinowski, W. Minor, "Processing of X-ray Diffraction Data Collected, in Oscillation Mode", *Methods in Enzymology*, vol. 276: Macromolecular Crystallography, part A (Eds.: C. W. Carter Jr., R. M. Sweet), Academic Press, New York, p. 307–326, **1997**.
[13] A. L. Spek, *J. Appl. Crystallogr.* **2003**, *36*, 7–13.
[14] G. Sheldrick, SHELXS-97, *Program for the Solution of Crystal Structures*, University of Göttingen, **1997**; G. M. Sheldrick, SHELXL-97, *Program for the Refinement of Crystal Structures*, University of Göttingen, **1997**.
[15] M. Lucas, P. Claus, *Chem. Ing. Tech.* **2001**, *73*, 252–257.
[16] M. van Schilfgarde, T. A. Paxton, O. Jepsen, O. K. Andersen, G. Krier, *Programm TB-LMTO*, Max-Planck-Institut für Festkörperforschung, Stuttgart, **1994**.
[17] U. Barth, L. Hedin, *J. Phys. Chem.* **1972**, *5*, 1629–1972.
[18] O. Jepsen, O. K. Andersen, *Z. Phys. B* **1995**, *97*, 35–37.
[19] A. D. Becke, E. J. Edgecombe, *Chem. Phys.* **1990**, *92*, 5397–5403.
[20] A. Savin, A. D. Becke, J. Flad, R. Nesper, H. G. von Schnering, *Angew. Chem.* **1991**, *103*, 421–424; *Angew. Chem. Int. Ed. Engl.* **1991**, *30*, 409–412.
[21] B. Silvi, A. Savin, *Nature* **1994**, *371*, 683–686.
[22] A. Savin, R. Nesper, S. Wengert, T. F. Fässler, *Angew. Chem.* **1997**, *109*, 1892–1915; *Angew. Chem. Int. Ed. Engl.* **1997**, *36*, 1809–1832.
[23] R. F. W. Bader, *Coord. Chem. Rev.* **2000**, *197*, 71–94.
[24] R. Dronskowski, P. E. Blöchl, *J. Phys. Chem.* **1993**, *97*, 8617.

Received: April 4, 2006
Published Online: July 27, 2006

